

A STATISTICAL APPROACH TO FRACTURE TOUGHNESS MODELING OF MA957 USING A σ^* - A^* CONCEPT—W. J. Yang, M. J. Alinger, T. Yamamoto, and G. R. Odette (University of California, Santa Barbara)

OBJECTIVE

The objective of this study was to model the fracture toughness of MA957 in the cleavage transition with a modified critical stress-critical stressed area (σ^* - A^*) model to gain insight on the mechanisms leading to the highly anisotropic fracture properties and the very low toughness for crack with fracture planes containing directions parallel to the extrusion direction.

SUMMARY

We modeled the temperature (T) dependent fracture toughness $K_{Jc}(T)$ of MA957 based on a statistically modified critical stress-critical stressed area (σ^* - A^*) concept. The finite element (FE) method was used to simulate the stress-strain fields as a function of the applied loading K_J at different T in terms of the area (A) encompassed by a specified normal stress contour (σ). Ideally the critical stress (σ^*) is defined by the point of intersection of $A(\sigma)$ plots at various T. However, a statistically mediated range of A^* was recognized in our model, corresponding to the intrinsic distribution of K_{Jc} : thus the point at which the $A(\sigma)$ at various T experience the maximum number of intersections was used to define σ^* . The fracture toughness of MA957 is strongly dependent on the specimen orientation. Analysis of cleavage initiation in the L-R orientation, with the highest K_{Jc} yielded the highest $\sigma^* \approx 3600$ MPa. In contrast, the σ^* for the C-L orientation, with the lowest K_{Jc} , yielded the lowest $\sigma^* \approx 2850$ MPa, while for the C-R orientation with intermediate K_{Jc} , $\sigma^* \approx 3000$ MPa. In the latter two cases, the ligament planes contain directions parallel to the extrusion direction. However, the A^* were roughly similar for all orientations ranging from ≈ 30 to $400 \mu\text{m}^2$. This is probably a result of a common distribution of cleavage initiation sites in the form of μm -scale Al_2O_3 particles aligned in the extrusion direction. The A^* - σ^* , was used to model median $K_{Jc}(T)$ and the corresponding curves at high and low fracture probabilities determined from a Weibull analysis. The model is in good agreement with previously measured K_{Jc} data, but requires a K_{min} of $10 \text{ MPa}\sqrt{\text{m}}$ in the C-L orientation, which less than the standard Master Curve (MC) value of $20 \text{ MPa}\sqrt{\text{m}}$. We conclude that the low toughness direction is due to both intrinsic crystallographic and microstructurally mediated factors.

PROGRESS AND STATUS

Introduction

Iron-chromium based alloys, strengthened with a high number density of nanometer-scale yttrium-titanium-oxygen clusters (NCs) have demonstrated outstanding high temperature creep strength [1]. Mechanical alloying (MA) ferritic powders with Y_2O_3 and Ti by high-energy ball milling, followed by consolidation at elevated temperature produces nm-scale, coherent Y-O-Ti solute clusters (NCs), as well as a more typical fine-to-coarser scale incoherent dispersed oxide particles [2,3]. We refer to these materials as nanostructured ferritic alloys (NFAs). The NCs are generally believed to be responsible for the high creep strength of NFAs. This high strength, coupled with high corrosion resistance, offers great promise for elevated temperature applications to fusion and advanced fission structures [4,5]. However, a challenge in the development of these alloys is maintaining adequate fracture toughness in combination with the high creep strength. Low toughness is a potential problem with these alloys since, in common with other BCC alloys, NFAs exhibit a ductile-to-brittle fracture mode transition over a characteristic range of T; and the very high strength of NFAs would be expected to result in decreased toughness relative to that of conventional steels.

We have previously characterized the tensile and fracture toughness of as-hot extruded NFA MA957, showing that this alloy has highly anisotropic properties and very low fracture toughness in the C-L and C-R orientations [6]. MA957 is hot extruded at 1150°C resulting in both anisotropic grains ($\approx 0.5 - 5 \mu\text{m}$) elongated in the extrusion direction and crystallographic texturing. Further Al_2O_3 impurity inclusions are

aligned as stringer particles in the extrusion direction. Thus a basic understanding of the micromechanical mechanisms controlling cleavage fracture, and how they relate to the underlying alloy structures, is critical to developing NFAs with adequate toughness. Three possible explanations for the anisotropy in the fracture properties and low toughness are proposed: 1) impurity alumina (Al_2O_3) particles from the ferrochrome powder source of the master alloy aligned in the extrusion direction provide geometrically favorable cleavage initiation sites; 2) the anisotropic grain size is effectively larger in the extrusion direction reducing the critical stress for microcracking; and 3) high degree of $(-11-1)[110]$ and $(-111)[110]$ crystallographic texture imparted by hot extrusion produces a intrinsically brittle cleavage orientation.

Experimental Procedures and FE Stress Field Simulations

The fracture toughness and tensile data for MA957 were reported in an earlier publication [6]. Fracture tests were performed at various temperatures on pre-cracked $a/W \approx 0.5$, $W = B/3$, Charpy sized (3.33x3.33x18.33 mm) bend bars in three orientations with respect to the extrusion direction shown in Fig. 1: L-R - longitudinal/length-radial crack plane; C-R - circumferential-transverse/length-radial crack plane; and C-L - circumferential-transverse/length longitudinal crack plane. The elastic and elastic-plastic $K_{Jc}(T)$ were evaluated in accordance with ASTM standard E 1921.

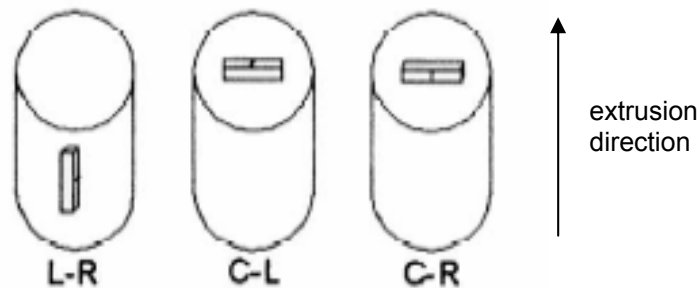


Fig. 1. The fracture specimen orientations reference to the extrusion direction.

Cleavage fracture initiates by the rapid propagation of a cleavage microcrack from a broken brittle cleavage trigger particle in the highly stressed volume ahead of the crack tip. Microcrack propagation requires a local critical Griffith type stress that depends on: a) the cracked particle size; b) its orientation with respect to the adjacent ferrite grain; and c) the corresponding orientation-dependent ferrite microcrack arrest toughness. The cleavage trigger particles are statistically distributed in size and orientation; thus specimen-to-specimen sampling variations lead to intrinsic scatter in K_{Jc} . The greater the stressed volume, $V = BA(\sigma)$, the higher the likelihood of activating a weakest link trigger particle leading to cleavage fracture. For this work, a modified critical stress-statistical stressed area (σ^*-A^*) concept was used to model $K_{Jc}(T)$ [7,8].

Plane strain 2D-FE calculations were used to simulate the stress distribution in front of a blunting semi-circular crack tip using the commercial ABAQUS code and the measured true stress-strain constitutive data fit to simple analytic functions. The quarter symmetry mesh was composed of 826 8-node isoparametric elements with a total of 2607 nodes. The mesh was highly refined crack tip with an initial radius of 1 μm . Post processing codes were used to evaluate $A(\sigma, T)$ for normal to yield stress ratios σ/σ_y from ≈ 2.4 to 3.6. Plots of $A(\sigma, T)$ versus σ were used to define σ^* for each orientation.

Results and Discussion

Figure 2 shows the $A(\sigma, T)$ versus σ . Recognizing that the K_{Jc} data are statistically distributed, we defined σ^* at the point of the maximum number of intersections of the $A(\sigma, T)$ curves. The A^* - σ^* varied with orientation, as shown by the vertical lines in Fig. 2. In the L-R orientation (Fig. 2a) $\sigma^* \approx 3600$ MPa, while $\sigma^* \approx 2850$ MPa in the C-L orientation (Fig. 2b) and $\sigma^* \approx 3000$ MPa (Fig. 2c) in the C-R orientation. The fracture toughness was found from $A(J = J_c) = A^*$ trajectories for each orientation. The cleavage fracture probability, F , for a three-parameter Weibull distribution is:

$$F = 1 - \exp\left[-\left(\frac{K_{Jc} - K_{min}}{K_0 - K_{min}}\right)^4\right] \quad (1)$$

Here K_{min} is the minimum fracture toughness and K_0 is the K_J at $F = 0.632$. The points labeled a are for a high F , while those labeled c are for a low F . The intermediate points, labeled b, was taken as the nominal median value of K_{Jc} at $F = 0.5$. The values of A^* for a, b, and c and the various orientations are summarized in Table 1.

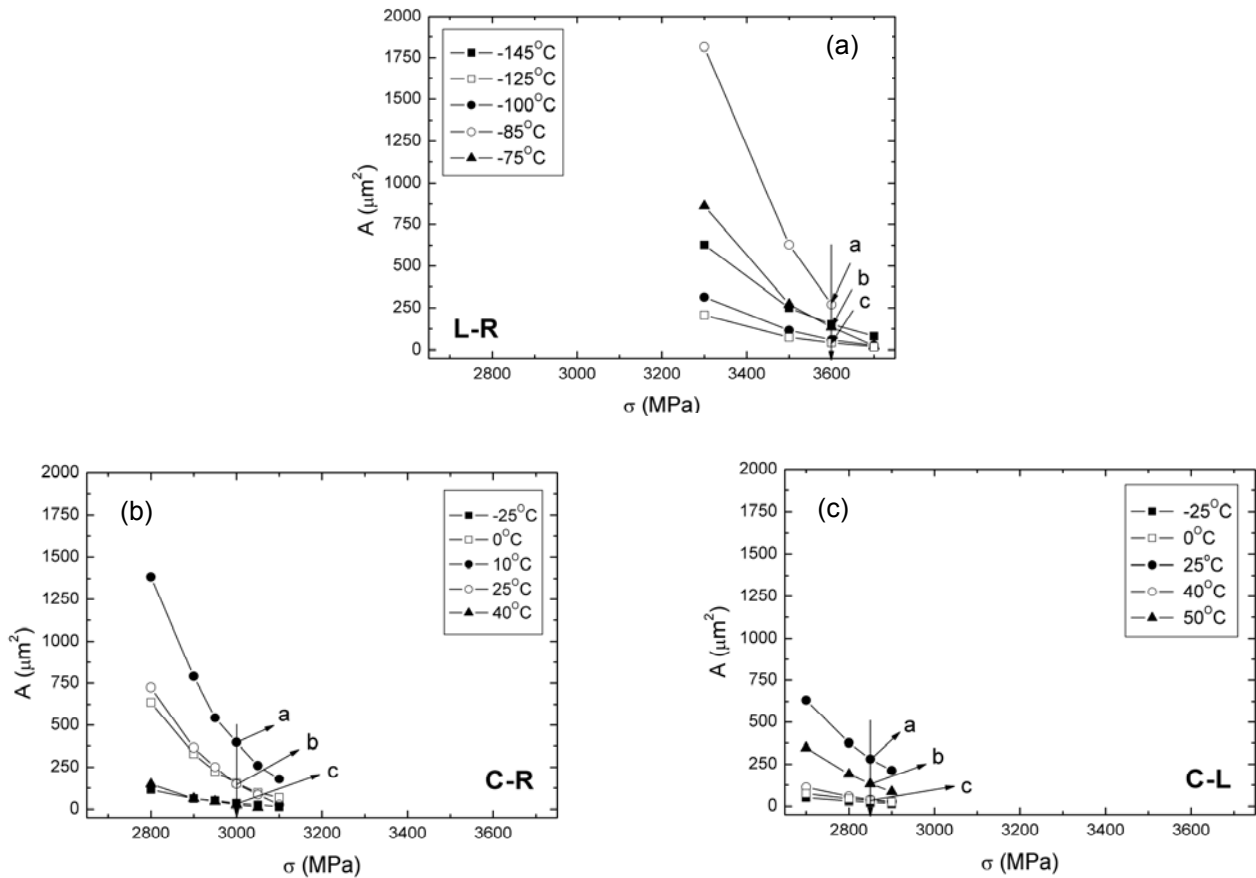


Fig. 2. The $A(\sigma, T)$ versus σ for each orientation and the points of maximum intersection defining σ^* (lines) for: (a) L-R; (b) C-R, and (c) C-L.

Table 1. The local σ^* (MPa) and A^* (μm^2) for cleavage fracture properties for each orientation

	σ^* , MPa	A^* for a	A^* for b	A^* for c
L-R	3600	270	144	49
C-R	3000	397	151	29
C-L	2850	281	132	30

The corresponding $K_{Jc}(T)$ curves cleavage for a, b, and c are shown in Fig. 3 along with a master curve for comparison. As shown in Fig. 3a, the data for the L-R orientation is consistent with $K_{min} = 20\text{MPa}\sqrt{\text{m}}$ with the high (a) and low (c) fracture probability curves falling at $F = 0.89$ and 0.09 , respectively. A $K_{min} = 20\text{MPa}\sqrt{\text{m}}$ also provides a reasonable fit to the C-R data shown in Fig. 3b, with the a and c points falling at $F = 0.98$ and 0.01 , respectively. However, fitting the C-L data (Fig. 3c) requires a lower $K_{min} = 10\text{MPa}\sqrt{\text{m}}$ with the a and c points falling at $F = 0.97$ and 0.07 , respectively. These results suggest modified σ^* - A^* models and the master curve (MC) concept can be applied to NFAs.

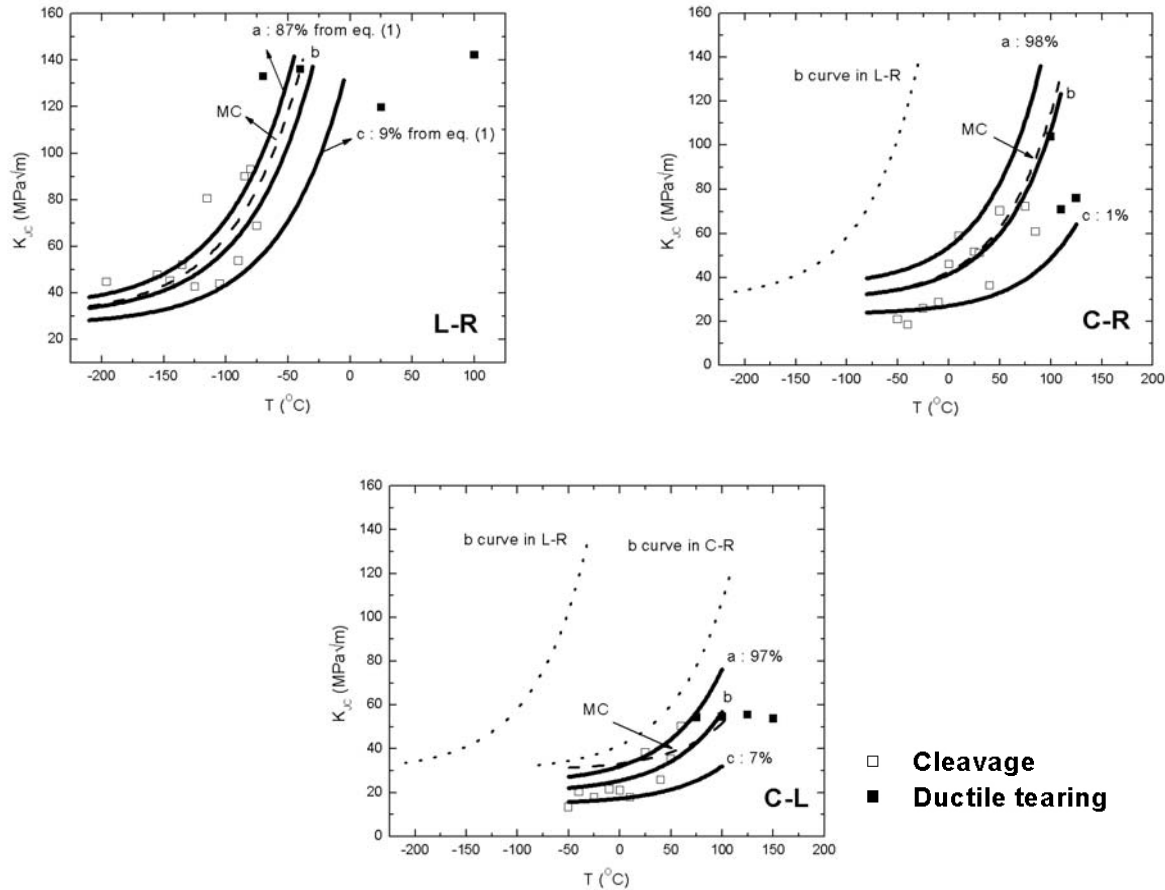


Fig. 3. Predicted $K_{Jc}(T)$ curves for the σ^* - A^* model for the median and specified fracture probability (F) conditions for the: a) L-R; b) C-R, and c) C-L orientations.

Discussion - The Physical Basis for Anisotropic and Low Toughness Orientations

The model-based analysis of the MA957 fracture data provides new insight regarding the challenges facing developing NFAs with adequate fracture toughness. We had previously argued that the low toughness in the C-L and, to a slightly lesser extent, in the C-R orientations was due to the stringers of impurity Al_2O_3 particles aligned in the extrusion direction. Thus if this were the sole reason for low toughness, the challenge would simply be to develop cleaner, inclusion free alloys. However this explanation does not rationalize the high toughness in the L-R direction which, as illustrated in Fig. 4a, is at least partially due to the tendency of the cracks to diverge out of the nominal ligament crack plane. This is in contrast to the planar cleavage fracture surfaces in the C-R and C-L orientations shown in Figs. 4b and c. The torturous fracture path in the L-R orientation results in higher K_{Jc} , but the underlying reason for the out-of plane cracking is likely due to the existence of an easy cleavage system oriented for crack propagation in the extrusion direction due to texturing.

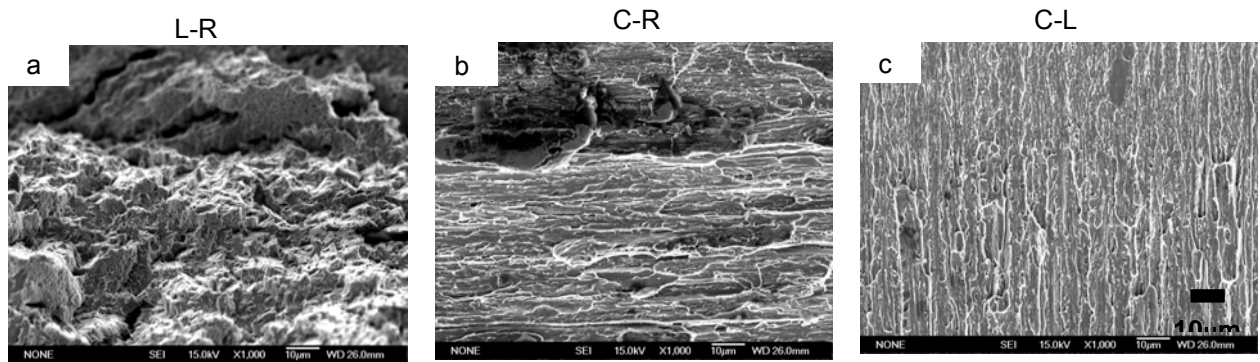


Fig. 4. Fracture surfaces for the: a) L-R; b) C-R; and c) C-L orientations.

Figure 5 schematically illustrates the concept of crack propagation on the easy cleavage system, which is the (100) plane in [010] and [011] directions in ferrite, and trigger particle-effective grain size effects. More detailed crystallographic descriptions along with quantitative analysis of the microstructure σ^* relations will be given in future reports. The particle-stringer and elongated grain orientations are shown by the colored elliptical (C-R and C-L) and circular (L-R) shaped symbols. The easy cleavage plane is shaded with blue and the ligament fracture plane in grey. Qualitatively, the larger grain particle and grain dimensions in the C-L orientation in the direction of crack propagation are expected to lead to the lowest σ^* . While the effective scale of the microstructure is smaller, the C-R orientation still has access to the easy cleavage system in with a extrusion direction lying in the ligament plane, thus has an intermediate σ^* . However, in the L-R orientation the cracks must kink out of the ligament plane to access the easy cleavage system. In combination with the smallest effective microstructure size, this leads to the highest σ^* . The strong tendency for propagation in the extrusion direction is shown in Fig. 6 for cracks produced by Knoop microhardness indentations at -196°C .

If verified by additional research, these concepts have important implications to the potential to develop NFAs with a combination of high strength and adequate toughness. In particular, while the clean alloy, inclusion and carbide free approach is still attractive extruded product form may still have intrinsically low toughness due to the presence of elongated grains and crystallographic texturing. The toughness may be improved with equiaxed and randomly oriented grains in HIPed product forms, but may still be limited by high levels of alloy strength.

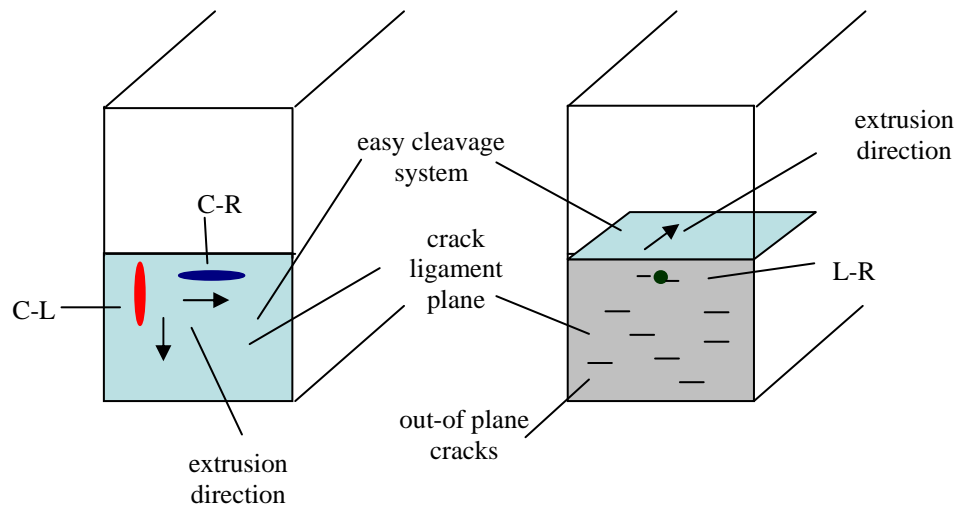
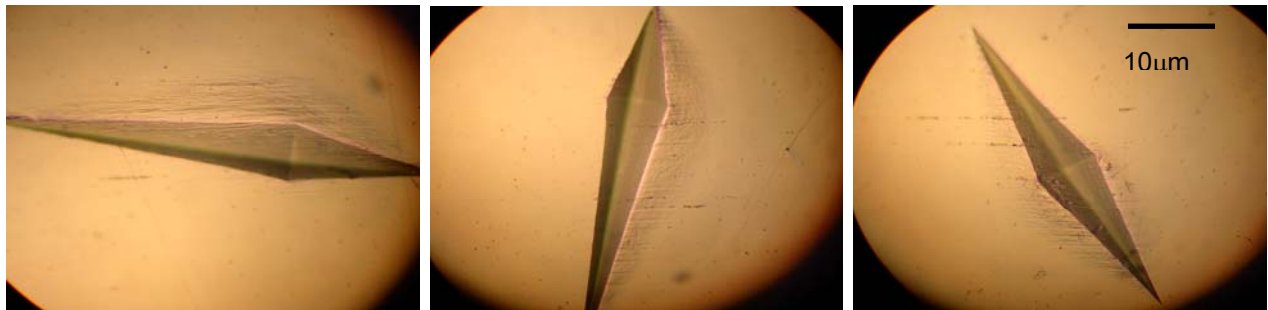


Fig. 5. Schematic illustration of the possible mechanisms leading to the strong orientation dependence and low values of C-R and especially C-L K_{Jc} .



→ ED

Fig. 6. Microcracks produced by various Knoop hardness indentations at -196°C , all propagating in the extrusion direction.

Future Research

The validity of the concepts proposed in this report will be evaluated in detail in future studies, including:

TEM assessments of the fracture surface crystallographic orientations, trigger particle sites and dislocation structures on FIBed specimens taken from the crack tip process zone.

Confocal microscopy quantification of the topology of the fracture surfaces and corresponding fracture reconstruction studies of initiation sites.

Analysis of the alumina inclusion size, shape, and orientation distributions.

Quantitative analysis of the relationship between the trigger particles, crack tip stress fields, and ferrite micro-arrest toughness.

Analysis of fracture toughness in simple Fe and model NFAs alloys produced by HIPing and hot extrusion.

Acknowledgements

The authors would like to thank Dr. D. Gelles of PNNL for supplying the MA957 and would like to acknowledge D. Gragg and M. L. Hribernik of UCSB for their experimental assistance and valuable discussion.

References

- [1] S. Ukai, M. Harada, H. Okada, M. Inoue, S. Nomura, S. Shikakura, K. Asabe, T. Nishida, and M. Fujiwara, *Nucl. Mater.* 204 (1993) 65.
- [2] T. Okuda and M. Fujiwara, *J. Mater. Sci. Lett.* 14 (1995) 1600.
- [3] M. J. Alinger, G. R. Odette, and D. T. Hoelzer, *J. Nucl. Mater.* 329–333 (2004) 382.
- [4] J. J. Fisher, US patent 4,075,010, Dispersion Strengthened Ferritic Alloy for use in Liquid Metal Fast Breeder Reactors (February 21, 1978).
- [5] G. D. Smith and J. J. deBarbadillo, in J. J. deBarbadillo et al. (eds.), *Structural Applications of Mechanical Alloying*, International, Materials Park, Ohio (1994) 117.
- [6] M. J. Alinger, G. R. Odette, and G. E. Lucas, *J. Nucl. Mater.* 307–311 (2002) 484.
- [7] H. J. Rathbun, G. R. Odette, M. Y. He, G. E. Lucas, and T. Yamamoto, NUREG/CR-6790.
- [8] G. R. Odette, T. Yamamoto, H. J. Rathbun, M. Y. He, M. L. Hribernik, and J. W. Rensman, *J. Nucl. Mater.* 323 (2003) 313.